IEEE Access
Multidisciplinary ⋮ Rapid Review ⋮ Open Access Journal

Received 25 May 2023, accepted 7 June 2023, date of publication 19 June 2023, date of current version 22 June 2023.

Digital Object Identifier 10.1109/ACCESS.2023.3287497

RESEARCH ARTICLE

Dual Ionic Transport Using Ca^{2+} and Na^{+} Signaling for Molecular Communication Systems

CARLOS DANILO MIRANDA REGIS[1], ÍTTALO DOS SANTOS SILVA[1], PEDRO IVO ARAGÃO GUIMARÃES[1], EMANUEL THIAGO DE ANDRADE DA SILVA[1], AND MICHAEL TAYNNAN BARROS[2], (Member, IEEE)

[1]Federal Institute of Education, Science and Technology of Paraíba, João Pessoa 58000-000, Brazil
[2]Unconventional Communications and Computing Laboratory, School of Computer Science and Electronics, University of Essex, CO4 3SQ Colchester, U.K.

Corresponding author: Carlos Danilo Miranda Regis (danilo.regis@ifpb.edu.br)

This work was supported in part by Fundação de Amaparoá Pesquisa do Estado da Paraíba (FAPESQ-PB) under Grant 07/21.

ABSTRACT Astrocytes have the ability to modulate neuronal communication by regulating various levels of ionic concentrations. The development of models for molecular communication ought to investigate the utilisation of various ionic transportation mechanisms, with the aim of enhancing performance and biocompatibility, thereby facilitating co-existence within cellular tissues. In this study, we suggest the utilisation of both Ca^{2+} and Na^{+} ions to investigate the non-linearities of propagation in cellular tissues for MC. In this study, we also investigated the impact of various ionic transport mechanisms, including the sodium-calcium exchanger, sodium-potassium pump, and calcium pump, to assess their impact on the intracellular propagation of Ca^{2+}. We analysed four communication metrics metrics, namely channel capacity, bit error rate (BER), communication gain, and signal-to-noise ratio, to evaluate the effects of the transport mechanisms on the communication channel.

INDEX TERMS Calcium signaling, ion transport structures, molecular communication system, molecular signals propagation.

I. INTRODUCTION

Calcium is one of the most important ions in neural tissues. Intercellular propagation of calcium molecules, or intercellular Ca^{2+} signalling, plays an essential role in the electrical excitability of central nervous system cells, such as astrocytes [1]. However, Ca^{2+} works non-linearly with other ions. One of the most influential ion to Ca^{2+} is sodium (Na^{+}) and their relationship is not only used for communication, but for maintaining transients that influence neural activities [2]. Compared to Ca^{2+}, in astrocytes, Na^{+} has higher values of intracellular and extracellular concentrations, in the order of mM (millimoles) differing in the spatial and temporal patterns characteristic of their signals [3]. The dynamics of variations in the concentration of Na^{+} in the cytosol (Na^{+} signal) considerably affect the behavior of other molecules, triggering a definitive process for the homeostasis of astroglial cells, a process by which astrocytes tend to remain in ionic equilibrium [4].

In Molecular Communications (MC), Ca^{2+} signalling and, more specifically, astrocytes have been recently studied [5], [6], [7]. While the majority of approaches have been computational [8], [9], [10], a few works in the field have investigated experimental outcomes in neuron-astrocyte communication scenarios [11], [12]. There are numerous biological phenomena that are not accounted for and that have an effect on both the digital structural and activity representations [13], [14]. Computational methods are not yet fully developed. Moreover, computational models need to include ionic transport relationships that are also known but have not yet been modelled, including the Ca^{2+} and Na^{+} signalling. Moving towards a more comprehensive and biologically plausible computational model is technically difficult, but it is the next step in solidifying the biological realism of molecular communications models. Thus, considering the contribution of Ca^{2+} and Na^{+} signalling in computational models of molecular communication allows

The associate editor coordinating the review of this manuscript and approving it for publication was Rajeswari Sundararajan.

increasing the accuracy of the ion transport process between astrocytes during the simulation since it also enables the implementation of regulatory structures that encourage the control of the concentrations of these molecules across the membrane [15].

In this paper, we develop communication system model for molecular communication system within astrocytes based on the dual ionic transport of Ca^{2+} and Na^{+} molecules. We consider several models of transport including the Na^{+} and Ca^{2+} Exchange Channel. (NCX), the Na^{+} and k^{+} Pump (NKP) and the Ca^{2+} Pump (CP) on the propagation of the Ca^{2+} signal in between. This model takes into account the variability of diffusion-based processes through a stochastic algorithm developed from the work of [16], which also enabled the implementation of the reactions of the three main ionic transport structures present in the plasma membrane. They are fundamental for astrocyte homeostasis to ensure greater precision in transmitting information between glial cells [17], [18].

The main contributions of this work are:

- Development of a **molecular communication system in astrocytes** based on the dual signalling of Na^{+} and Ca^{2+}.
- Evaluation of **structural effects of ionic transport (NCX, NKP and CP)**.
- Analysis on the performance of the molecular communication system in terms of **channel gain**, **channel capacity**, **bit error rate (BER)** and **signal to noise ratio (SNR)**.

Our method hope to show improvements in biological realism for molecular communications but we also show the next building blocks for tunable molecular communications inside cellular tissues. We add more robustness to the computational models present in the literature while increasing complexity, appropriating actual biological structures and concepts [19]. The dual ionic modes initiate an unexplored solution in MC that shows how the influence of different molecules and ionic structures is essential for the process of communication between the astrocytes, as well as providing a relevant analysis regarding cellular communication in neural biological systems.

II. RELATED WORKS

Ca^{2+} signalling models for molecular communications has been studied in many tissue types including epithelial and smooth muscle tissues, based on the methodology described in the work of [20] and [21], was presented by [22]. Still, the main contribution of [22] was the analysis of communication between astrocytes based on diffusion through gap junctions [23], in which the influence of the spatial-temporal dynamics of Ca^{2+} concentration in the intracellular signaling process, molecular diffusion delay, communication gain, and channel capacity. Although the communication network between the astrocytes showed a more uniform distribution of the Ca^{2+} concentration in the cells of the other tissues, it also returned a lower communication gain, between -65 dB to -88 dB, smallest channel capacity for the shortest distances between Tx and Rx (< 0.025 bits).

A computational model for understanding how an astrocyte network based on Ca^{2+} signaling regulates its concentration levels in healthy tissue and tissue affected by Alzheimer's disease was implemented by [16]. To evaluate terms of communication gain, molecular delay, and propagation range, the effects of the propagation dynamics of the β-amyloid plates in different topologies of the [24] network. The channel gain values obtained for the regular grade topology ranged from about -22 dB to about -35 dB in healthy tissue, while there was a variation of -25 dB for -50 dB in the pathological tissue. However, both declined exponentially along the communication channel.

None of these works considered the influence of Na^{+} signaling, whose homeostatic reactions play a fundamental role in the development of several functions of central nervous system cells [4], [25], [26]. According to [27], in neurons, the generation of action potentials requires a large ionic concentration of Na^{+}, while the stimulation of astrocytes from neurotransmitters considerably increases the concentration of this ion in the cytosol ($[Na^{+}]_i$). In addition, transients of $[Na^{+}]_i$ are also influenced by ionotropic glutamate receptors, Bergmann glial cells, and hippocampal astrocytes, promoting the propagation and transport of molecules between cells and across the membrane [3].

The concentrations of sodium and calcium in the cytosol of astrocytes are fundamentally regulated by diffusion through the ionic transport channels present in the plasma membrane, such as the Sodium and Calcium Exchange Channel (NCX), the Sodium and Potassium Pump (NKP), and the Calcium Pump (CP) [3], [4]. Investigated the role of sodium signaling on the perisynaptic processes of [28] astrocytes mediated by calcium signaling through NCX operation [15]. This work indicated that the action of short duration $[Na^{+}]_i$ pulse in the communication system, through the NCX, can prolong and amplify the intercellular signal of Ca^{2+} (variations in the intracellular concentration of Ca^{2+}) in a non-linear way up to 0.1 μM (micromol), approximately, depending on the amplitude of the transients of Na^{+} (15 mM$-$35 mM).

The Na^{+}/k^{+} pump was investigated by [29], who carried out an analysis of its working principle to characterize the ionic currents arising from k^{+} transients [30], [31], as well as the chemical reaction and kinetic properties associated with the passage of this ion through the walls of the bomb, compared to the Na^{+} ion. Using a high-speed voltage clamp circuit and giant squid axons, the authors were able to characterize the ionic bonds involving the transport of 1 mM extracellular k^{+}, observing the behavior of the relaxation charge and found that the electrical signals caused by the ordered movement of k^{+} ions through the pump are smaller in amplitude (about 5 times) and faster ($\approx$10 times).

Reyes et al. [32] evaluated the control of $[Na^{+}]_i$ and $[Ca^{2+}]_i$ (intracellular concentrations of sodium and calcium, respectively) through the action of the NCX, the NKP and

Ca^{2+} Pump in astrocytes from rat cortex in two states: resting and stimulated, in order to understand the primary influence of these signals on glutamate transmission and control of glial cell metabolic signaling [33]. The authors came to the conclusion that the three transport structures are elementary agents in the homeostasis of Na^{+} and Ca^{2+} ions in both states, with CP being the main emitter of Ca^{2+} for the extracellular medium, while the NCX is the most relevant in the introduction of this ion into the cytosol and the NKP assuming the predominance in the elevation of the extracellular signal of Na^{+} ($[Na^{+}]_o$).

In our paper we propose a new molecular communication model considering the advantages of adding Na^{+} signaling to the communication system between astrocytes developed by [22], as well as the reactions from NCX, NKP, and CP, increasing the complexity of computational models of molecular communication based solely on Ca^{2+} signaling present in the literature. In addition, the challenges and implications of implementing these structures and evaluating the overall performance of the system, in terms of communication gain, bit error rate, channel capacity, and signal-to-noise ratio, are also the purpose of the present work.

III. Na^{+}/Ca^{2+} SIGNALLING MECHANISM

Astrocytes are crucial CNS cells interacting with other elements and processes in a two-way communication system. The activation of gap junctions in astrocytes is directly influenced by frequent fluctuations in ion concentrations and the ionic flux generated in the diffusion of Ca^{2+} and Na^{2+} molecules, with diffusion occurring when both the connexons are in high conductance open state [34].

Analogously to the signaling of Ca^{2+}, the signaling of Na^{+} occurs intracellularly and extracellularly. The baseline for the concentration of Na^{+} in the cytosol of astrocytes (when the cell is at rest) is around 15−20 mM. But electrical stimulation on a single astrocyte can produce a volume concentration of this ion about 10−25 mM above this [35], [36] baseline.

The astrocytes that receive the stimulus also suffer the effect, further suggesting that the propagation of sodium signals happens radially to all surrounding cells, following the dynamic model of diffusion [37], [38], which favors the dissipation of the high concentration of Na^{+}, restoring initial baseline levels.

Among the structures to which the Na^{+} signals in astroglia are linked, we can highlight, in particular, the sodium-potassium pump (NKP) and the Na^{+}/k^{+} transporter channel. In addition, cl^{-}, which also regulate the storage of k^{+}, and the sodium and calcium exchange channel (NCX), whose activities are directly controlled by $[Na^{+}]_i$ [3]. NKP is the primary external energy-dependent Na^{+} transporter in astrocytes, through which increased neuronal activity triggers lactic acid synthesis. At the same time, NCX is the most physiologically important ion exchange channel whose action directly modulates the signaling of Ca^{2+} [39].

A. CHANNEL EXCHANGE OF Na^{+} AND Ca^{2+}

The NCX is an unique mechanism that allows the output of Ca^{2+} against its ionic gradient without consuming external energy but obtaining power through the change in the electromechanical angle of the membrane with the entry of Na^{+} [40]. The modes of operation of NCX can be switched with each other through changes in these electromechanical gradients of Na^{+} and Ca^{2+} and in the membrane potential (V_m), which are also consequences of the operation of the different ionic transport structures present in the plasma membrane [33], [41]. In astrocytes, the NCX reversal potential, that is, the potential at which dynamic switching between modes of operation occurs, is close to the resting membrane potential, which is approximate −80 mV [42], [43].

The reverse mode is internally dependent on $[Na^{+}]_i$ for the input of Ca^{2+} and externally dependent on $[Ca^{2+}]_o$ (extracellular concentration of Ca^{2+}) for the output of Na^{+}. However, NCX considers the Ca^{2+} concentrations in the cytosol as a critical requirement for activating either of the two [44] modes of operation. For squid axon cells and cardiomyocytes, for example, $[Ca^{2+}]_i$ must be on the order of 1μM so that only in a small part of the cells is the NCX active in sleep mode ($[Ca^{2+}]_i = 100$ nM). Activation also occurs with a low external concentration of Na^{+}, so as $[Na^{+}]_o$ increases, the flux of Ca^{2+} to the cytosol decreases [45].

The direct mode is externally dependent on $[Na^{+}]_o$ for the output of Ca^{2+} and internally dependent on $[Ca^{2+}]_i$ for the input of Na^{+}. This mode is also activated by the intracellular concentration of Ca^{2+}, causing the NCX exchange process to be considered asymmetric since the direct method does not depend on $[Ca^{2+}]_o$ for its activation [44]. Depolarization and increase in $[Na^{+}]_i$ favor switching to reverse mode, while the rise in $[Ca^{2+}]_i$ favors forward mode [3], [15]. NCX operates in reverse mode in cultured cortex astrocytes even under resting conditions [32], [33].

B. Na^{+} SIGNALING MODEL

The flow of Na^{+} and Ca^{2+} molecules through the NCX structure causes an electrogenic transport, that is, a net movement of charges (ions) across the membrane, which can be measured as an ionic current, from which the value of the flux [46] is estimated. This exchanger channel ion flow Na^{+}/Ca^{2+} (J_{NCX}), then describes the traffic of Ca^{2+} transients under the influence of electromechanical components of the reaction through the effects of the Na^{+} gradient and the action of the membrane potential, known as the Ca^{2+} NCX flux mediated by Ca^{2+} [15], [47]. Equation 1 expresses the J_{NCX} for both modes of operation for a discrete-time k, which corresponds to the mathematical modeling used to control intracellular and extracellular concentrations of Na^{+} and Ca^{2+} via the NCX in the cell [22], [20]:

$$J_{\mathrm{NCX}}[k] = G_{NCX} \cdot \frac{[Ca^{2+}]_i[k]}{[Ca^{2+}]_i[k] + C_{\mathrm{NCX}}} \cdot (v_m[k] - v_{\mathrm{NCX}}). \tag{1}$$

TABLE 1. Parameters for NCX ion flux calculation [20].

Parameters	Value	Unit
G_{NCX}	$3.160{\cdot}10^{-3}$	$\mu MmV^{-1}s^{-1}$
C_{NCX}	0.5	μM
v_{NCX}	-80	mV
R	$8,314472$	$Nmg^{-1}mol^{-1}K^{-1}$
T	$298,16$	K
m	2	-

G_{NCX} is the total cell conductance, expressed in $\mu MmV^{-1}s^{-1}$, C_{NCX} is the average concentration of Ca^{2+} for NCX activation [21], [20], v_{NCX} is the NCX reversal potential [3]. Finally, , v_m is the membrane potential, which the Nernst Equation can calculate, observed in Equation 2 [48]:

$$v_m[k] = 2,3 \cdot \frac{RT}{mF} \cdot \log_{10}\left(\frac{[Ca^{2+}]_o[k]}{[Ca^{2+}]_i[k]}\right), \tag{2}$$

in which R is the universal gas constant, T is the room temperature, and in Kelvin, m is the ionic charge of Ca^{2+}. Table 1 describes the parameter values used to calculate the J_{NCX}.

IV. COMPUTATIONAL MODEL OF A DUAL SIGNALLING COMMUNICATION SYSTEM

The computational model proposed by this work was adapted from the communication system designed by [16], which simulated a three-dimensional tissue of astrocytes where Ca^{2+} molecules are transmitted in the intracellular medium [49], characterizing itself, therefore, as a purely Ca^{2+} signaling system, whose reactions take place by a diffusion process based on gap junctions (GJ channels).

Figure 1 describes the basic flowchart of the entire system algorithm developed by this work. Initially, a stimulus is performed on the transmitting astrocyte (Tx), which is a square pulse of $[Ca^{2+}]_i$ of amplitude A and frequency f, necessary to excite the process of diffusion in the tissue. It is essential to point out that Ca^{2+} is the molecule considered most important for the communication system proposed by this work and, therefore, the variation in $[Ca^{2+}]_i$ is pointed out as the reference signal, from which the model evaluation metrics are based, to analyze the influence of the other reactions of the system on the Ca^{2+} signaling.

As seen also in Figure 1, the communication process starts with the signaling of Ca^{2+}. Then, the model of Na^{+} signaling happens through diffusion through the GJ channels in the intracellular medium, followed by the NCX and the NKP and CP pumps, which offer the exchange of molecules with the extracellular medium, activating $[Na^{+}]_o$, $[k^{+}]_i$, $[k^{+}]_o$ (extracellular potassium concentration) and $[Ca^{2+}]_o$. The models occur in this sequence, but their respective reactions are selected pseudorandomly through the stochastic algorithm, which also determines the astrocyte (not necessarily the same) in which each one must occur at that instant. This reaction is chosen based on its probability of occurrence (p_r) determined by the algorithm, which also calculates the execution time of the respective reaction (τ).

In this way, the next time instant of the system simulation ($t_s[k+1]$) is defined as the sum of the maximum execution time (τ_{max}) chosen among the reactions performed in the k iteration and the current $t_s[k]$, as noted in Eq.(3). Thus, while $t_s[k+1]$ does not reach the total simulation time (T_t), the process repeats itself from the input stimulus in Tx:

$$t_s[k+1] = t_s[k] + \tau_{\max}[k]. \tag{3}$$

Figure 2 illustrates the block diagram that describes this analysis, dividing the process into three parts: emission, channel, and reception, whose definitions are necessary to understand the proposed study.

A. EMISSION

To simplify, making the input pulse width of the system tend to an infinitesimal value, it can be said that the Tx is stimulated by a train of impulses of $[Ca^{2+}]_i$ ($S[k]$), of amplitude A and frequency f, described by Equation 4, where $l \in \mathbb{N}, l = 1, 2, \ldots, \lfloor \frac{T_t}{T} \rfloor$ and $T \in \mathbb{N}, T = \lfloor \frac{1}{f} \rfloor$. After the stimulus, a signal $X[k]$ is triggered from Tx by defining the reaction models in the channel. This signal is modulated and transmitted to the other tissue cells until it reaches the receptor astrocyte (Rx).

$$S[k] = A \cdot \sum_{l=0}^{\lfloor \frac{T_t}{T} \rfloor} \delta[k - l \cdot T] \tag{4}$$

1) MODULATION AND DETECTION

After the input stimulus induces the propagation of Ca^{2+} through Tx in the proposed communication system, the signal $X[k]$, which is a function of $[Ca^{2+}]_i$, undergoes a BCSK modulation process (Binary Concentration Shift Keying), which is analogous to ASK modulation (Amplitude Shift Keying). In this type of modulation, a symbol should be identified as bit 1 if the volume of intracellular concentration of Ca^{2+} transmitted by the cell during a specific time, or bit time (T_b), exceeds a predefined threshold concentration value (σ_0). Otherwise, it will be considered as a bit 0 [50]. Thus, a symbol can be coordinated to represent b bits simultaneously, using 2^b different concentration volumes with $2^b - 1$ threshold values. In the present work, it was defined that $b = 1$.

illustrates a section of the astrocyte tissue of the system in the plane xy in which the Tx and Rx are arranged, spaced by a distance r, in cells, after the stimulus of Ca^{2+} in Tx, diffusion starts, propagating $X[k]$ with a maximum amplitude of α. The volume of $[Ca^{2+}]_i$ transmitted every T_b second (C_b) must be compared to the threshold σ_0 to identify whether the sent bit is 0 or 1, returning the modulated signal $X^*[k]$, in bits.

When $X^*[k]$ propagates, considering that the molecules do not follow a defined path, but there is a diffuse scattering through the tissue due to the stochastic characteristic of the [51] system, it is necessary to carry out a signal

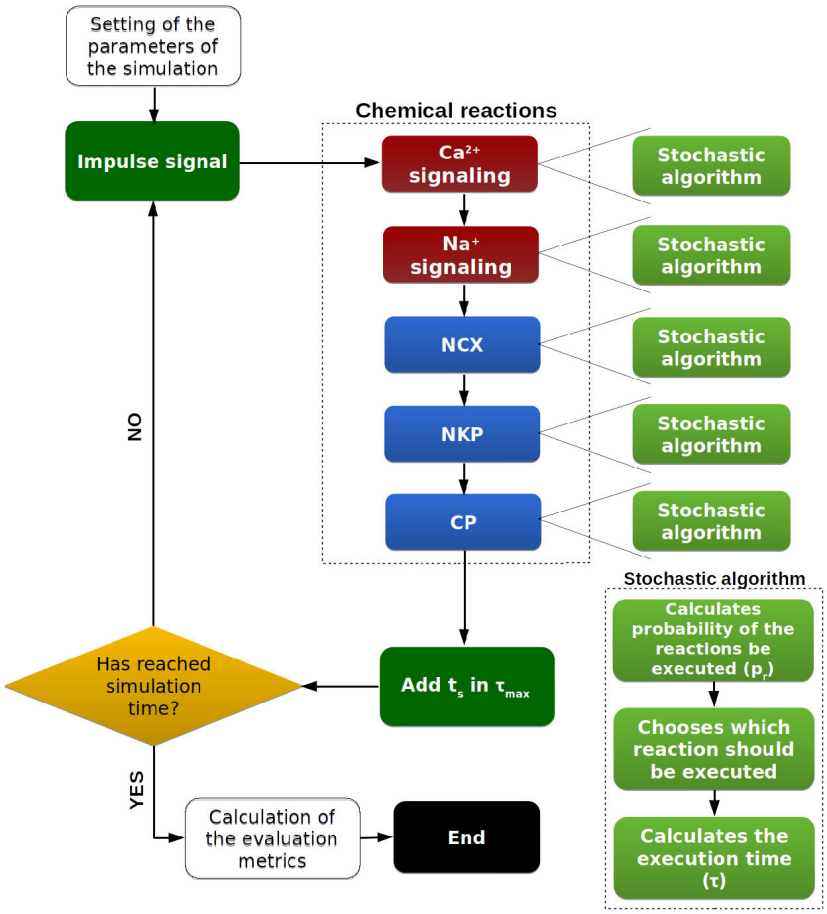

FIGURE 1. Basic flowchart of the computational model.

detection process to receive the information itself in the desired astrocyte. Thus, for the implementation of the model, assuming the coordinates x, y, and z to determine the position of the recipient cell in the tissue, a stochastic variable (H_{TxRx}) was defined that is directly proportional to the probability that the algorithm [52] chooses the reactions of Tx ($p_{Tx}(r_{Tx}, \tau_{Tx})$) and the reactions of at least one of the cells around Rx, as described in Equation 5. Thus, Equation 5 estimates the accumulated probability of a volume of information ($X^*[k]$) reaching and being detected by Rx so that communication is successfully established:

$$H_{\mathrm{TxRx}} \propto (p_{x-1,y,z} + p_{x+1,y,z} + p_{x,y+1,z} + p_{x,y-1,z} + p_{x,y,z+1} + p_{x,y,z-1}) \cdot p_{\mathrm{Tx}}(r_{\mathrm{Tx}}, \tau_{\mathrm{Tx}}). \quad (5)$$

For simplicity, the sum of the probabilities in Equation 5 was considered constant and, when multiplied by the proportionality constant necessary to establish equality, the term β is obtained, according to Equation 6, considered equal to 1 by the present paper:

$$H_{\mathrm{TxRx}} = \beta \cdot p_{\mathrm{Tx}}(r_{\mathrm{Tx}}, \tau_{\mathrm{Tx}}). \quad (6)$$

The quantity representing the system channel is then determined as a random variable Υ_{TxRx} (Equation 7), obtained from a distribution Gamma, with N_γ trials and probability of success p_γ, which simulates the characteristics of the diffusion of molecules through the tissue in intercellular communication, according to the works of [53] and [54]:

$$\Upsilon_{\mathrm{TxRx}} \triangleq \Gamma\left(\frac{\max[C_b]}{\alpha}, H_{\mathrm{TxRx}}\right). \quad (7)$$

Finally, Equation 8 demonstrates the demodulation of the detected signal ($Y[k]$), in bits, as a multiplication between the modulated signal and the random variable that represents the channel, following the method proposed by [55], ending the reception process:

$$Y[k] = \Upsilon_{\mathrm{TxRx}} \cdot X^*[k]. \quad (8)$$

B. THE CHANNEL

We consider the channel composition containing only the astrocytes tissue, including Tx and Rx, which has the medium previously determined in the simulation, that is, the selection of reaction models (signals of Ca^{2+} and Na^{+}, NCX, and the pumps), or combinations thereof, which will define how the signal will be propagated in the communication system. The keys c_1–c_5 in Figure 2 are merely illustrative to represent the choice of a combination of reaction models that must compose the channel by switching the open or closed states.

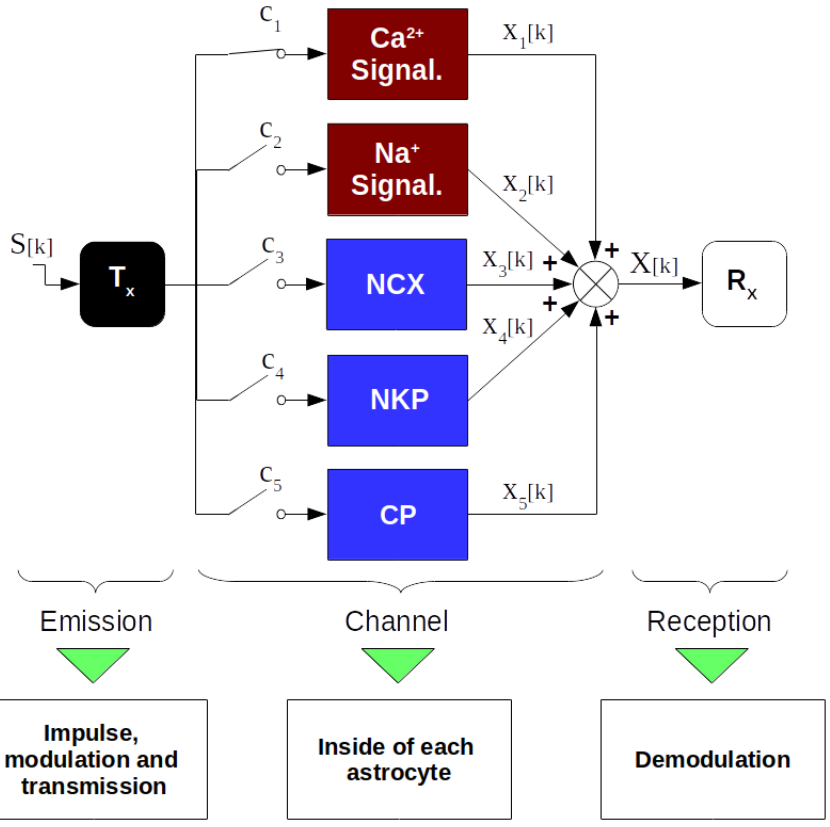

FIGURE 2. Block diagram of communication system analysis.

The astrocyte tissue is composed of 225 spherical cells distributed in a three-dimensional way so that the x axis has 15 cells, the y axis has five compartments, and the z axis has three cells. The Tx and Rx are positioned on the same plane xy, spaced by a distance r (given in cells) on the x axis. The astrocytes communicate according to their adjacencies in all directions, except for diagonals, in a topology known as a regular degree [24]. The choice of tissue structure, number of cells per axis, and communication topology was carried out according to the research addressed by [16], which is the reference model assumed by the present work.

C. RECEPTION

The $X[k]$ signal is a function of $[Ca^{2+}]_i$, which depends on the choice of the states of the keys c_1–c_5, according to Equation 9, which shows the resulting signal from the configuration of reaction models that we intend to analyze in the present work.

$$X[k] = \begin{cases} x_1[k], & \text{if } c_1 \text{ is closed.} \\ x_1[k] + x_3[k], & \text{if } c_1 \text{ and } c_3 \text{ are closed.} \\ x_1[k] + x_2[k] + x_3[k], & \text{if } c_1, c_2 \text{ e } c_3 \text{ are closed.} \\ x_1[k] + x_3[k] + x_4[k] + x_5[k], & \\ \quad \text{if } c_1, c_3, c_4 \text{ e } c_5 \text{ are closed.} & \\ x_1[k] + x_2[k] + x_3[k] + x_4[k] + x_5[k], & \\ \quad \text{if all switches are closed.} & \end{cases} \tag{9}$$

The signal $x_{\#}[k]$ as a "contribution of the reaction model # in $[Ca^{2+}]_i$", whose resulting variation represents the reference signal of the system ($X[k]$). That is, $x_1[k]$ is the contribution, or variation, caused by signaling Ca^{2+} in $[Ca^{2+}]_i$, $x_2[k]$ is the signaling contribution of Na^{+} in $[Ca^{2+}]_i$ and so on. Some reactions contribute directly, such as those from Ca^{2+} and CP signaling, and others contribute indirectly, that is, through the influence of other molecules, as is the case with other reaction models, so that all $x_{\#}[k]$ signs are defined in terms of $[Ca^{2+}]_i$.

The $X[k]$ signal is propagated within each astrocyte, being disseminated throughout the tissue. The Rx then performs the detection and subsequent demodulation of the signal in order to finish the reception process. The combinations described in Equation 9 were chosen because they sufficiently express the general objective of this master's thesis, which is to evaluate the influence of the proposed reaction models on Ca^{2+} signaling. In the simulation process, it was observed that the reactions from the NCX are curiously faster than the others. For this reason, the combination that describes the channel composed of NCX reactions and Ca^{2+} signaling (c_1 and c_3 close finish the reception process, was mainly analyzed to determine the proportion between the occurrences of a reference model.

Figure 3 illustrates the channel arrangement composed of the NCX structure (Figure 3 **c**) and the GJ channels (Figure 3 **d**), which allow flagging of Ca^{2+} and Na^{+}.

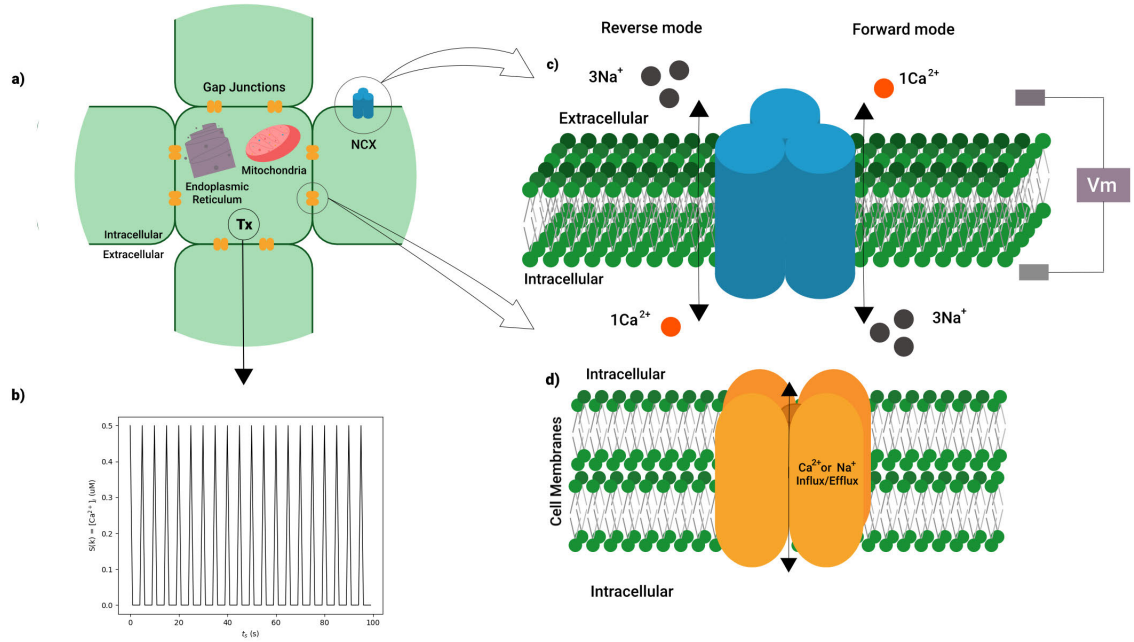

FIGURE 3. Molecular communication system developed. a) Cutting the astrocyte tissue around the Tx. b) Stimulus ($S[k]$) by pulses of $[Ca^{2+}]_i$ in the transmitting astrocyte. c) The NCX and its modes of operation. d) Communication via gap junctions for Ca^{2+} and Na^{+} signaling.

Furthermore, such an arrangement favors the propagation of the $X[k]$ signal after the input stimulus (Figure 3 **b**) in the transmitting astrocyte through the occurrence of reactions along with the tissue (Figure 3 **a**). In addition to these structures, the Na^{+}/k^{+} pump and the Ca^{2+} pump were implemented, constituting the molecular communication system developed in this work.

V. EVALUATION OF THE MOLECULAR COMMUNICATION SYSTEM

For the analysis of the computational model, the transport of Ca^{2+} molecules between the extracellular and intracellular media in any direction, that is, the variations in $[Ca^{2+}]_o$, is considered as a communication system noise, $g[k]$, because this variable directly influences, whether positively or negatively, the intracellular signal of Ca^{2+}, $X[k]$, which is the system reference signal. So that the variations in $g[k]$ represent the exit or entry of Ca^{2+} from the cytosol of any cell coming from or destined for the extracellular medium.

Thus, the SNR (Signal-to-Noise Ratio) is calculated, Equation 10, defined as the ratio between the intracellular signal energy of Ca^{2+} (E_{C_i}) and the energy of $g[k]$ (E_{C_o}), which represents the changes in $[Ca^{2+}]_o$:

$$\text{SNR} = 10 \times \log_{10}\left(\frac{E_{C_i}}{E_{C_o}}\right). \tag{10}$$

So E_{C_i} and E_{C_o} can be calculated according to Equation 11 and Equation 12, respectively:

$$E_{C_i} = \sum_{k=0}^{T_t} X^2[k], \tag{11}$$

$$E_{C_o} = \sum_{k=0}^{T_t} g^2[k]. \tag{12}$$

Another metric used to evaluate the system was the communication gain, defined as the gain in $[Ca^{2+}]_i$ and calculated as the ratio between the average concentration of Ca^{2+} in the cytosol of Rx ($\overline{C}_{i_{\text{Rx}}}$) and Tx ($\overline{C}_{i_{\text{Tx}}}$), according to Equation 13:

$$\text{Gain} = 10 \times \log_{10}\left(\frac{\overline{C}_{i_{\text{Rx}}}}{\overline{C}_{i_{\text{Tx}}}}\right). \tag{13}$$

To observe the channel capacity, $X^*[k]$ and $Y[k]$ are investigated to evaluate the fidelity between the two signals and the probability that the bits of information sent by the Tx arrive at Rx. For this, it is assumed that Tx and Rx are fully synchronized, a common consideration in the literature for high values of T_b [22], [56]. So, for each time of bit (T_b), both Tx and Rx will be alert about the transmission of bit in the middle, even if it doesn't reach Rx due to scattering in the [34], [57] channel.

Shannon entropy [58], $H(X)$, can represent the volume of information (in bits) in various processes of biological systems [59]. X and Y being the sets of possible states for the bits of Tx and the bits of Rx, respectively ($X = (0, 1)$, $Y = (0, 1)$) and p, the set of probabilities for Tx to send the bit x or Rx to receive the bit y, $H(X)$ can be calculated by Equation 14:

$$H(X) = -\sum_{x \in X} p(x) \cdot \log_2\left(p(x)\right). \tag{14}$$

Thus, the conditional entropy can be defined from the joint probability distribution and the conditional probability distribution of x and y:

$$H(X|Y) = -\sum_{x\in X}\sum_{y\in Y} p(x,y)\cdot \log_2\left(\, p(x|y)\,\right). \tag{15}$$

The other probabilities are obtained through Eqs. 16– 19:

$$p(x) = \begin{cases} p(x=0) & \text{or} \\ p(x=1) \end{cases} \tag{16}$$

$$p(y) = \begin{cases} p(y=0) & \text{or} \\ p(y=1) \end{cases} \tag{17}$$

$$p(y=0|x=0) = 1 - p(y=1|x=0), \tag{18}$$

$$p(y=0|x=1) = 1 - p(y=1|x=1). \tag{19}$$

The channel capacity is then determined by Equation 20, which describes the maximum value returned by the mutual information, obtained according to Equation 21, which determines the mutual dependence between the two variables x and y:

$$C(X;Y) = \max[I(X;Y)], \tag{20}$$

$$I(X;Y) = \sum_{y\in Y}\sum_{x\in X} p(x)p(y|x)\log_2\left(\frac{p(y|x)}{p(y)}\right). \tag{21}$$

Finally, the bit error rate (BER - Bit Error Rate) is calculated by comparing the signals $X^*[k]$ and $Y[k]$ according to the bits sent and received. So that the BER is obtained by the ratio between the number of bits received that do not correspond to those sent by Tx (B_{error}) and the total amount of bits sent (B_{total}), according to Equation 22.

$$\text{BER} = \frac{B_{\text{error}}}{B_{\text{total}}} \tag{22}$$

The system input parameters are defined at the beginning of the simulation, as illustrated in Figure 1, and are described in Table 2, as well as some model highlight variables. The adjusted value for A was 0.5 μM, which corresponds to the average oscillation amplitude of $[Ca^{2+}]_i$ in IP_3 channels, according to [60]. The baseline (LB) of the molecular concentrations of the system, that is, the initial values for $[Ca^{2+}]_i$, $[Ca^{2+}]_o$, $[\ Na^{+}]_i$, $[Na^{+}]_o$, $[k^{+}]_i$ and $[k^{+}]_o$ were defined as observed in Table 2.

VI. RESULTS

NCX promotes the exchange of Ca^{2+} and Na^{+} with the extracellular medium, causing a variation in the molecular concentration of this medium, which in turn influences the intracellular medium.

Observing the SNR curves plotted by changing the value of N_{NCX}, it is possible to analyze the direct influence of the NCX reactions on the $X[k]$ signal. Figure 4 shows the behavior of the SNR, calculated according to Equation 10, for each value of N_{NCX} chosen, over the frequency range (f) of the input stimulus ($S[k]$).

TABLE 2. Input parameters and some model variables.

Input Parameters		
Parameters	**Value**	**Reference**
A	0,5 μM	[60]
f	0,1−1 Hz	[16]
T_t	200 s	[16]
LB $[Ca^{2+}]_i$	0,1 μM	[22]
LB $[Ca^{2+}]_o$	10 μM	[42]
LB $[Na^{+}]_i$	15000 μM	[26]
LB $[Na^{+}]_o$	666 μM	[26]
LB $[k^{+}]_i$	140000 μM	[61]
LB $[k^{+}]_o$	4000 μM	[62]
α	0,01 μM	[22]
T_b	0,01−0,1 s	[54]
σ_0	$2\times\alpha$ (μM)	-
β	1	-
Important variables		
Variable	**Description**	
$x_1[k]$	Contribution of Ca^{2+} flag in $[Ca^{2+}]_i$ (μM)	
$x_2[k]$	Contribution of Na^{+} flag in $[Ca^{2+}]_i$ (μM)	
$x_3[k]$	Contribution from NCX in $[Ca^{2+}]_i$ (μM)	
$x_4[k]$	NKP contribution in $[Ca^{2+}]_i$ (μM)	
$x_5[k]$	CP contribution in $[Ca^{2+}]_i$ (μM)	
$X[k]$	Combination of models, depending on $[Ca^{2+}]_i$	
$X^*[k]$	$X[k]$ modulated (bits)	
C_b	Volume $[Ca^{2+}]_i$ transmitted during T_b s (μM)	
$Y[k]$	Signal received after detection (bits)	
$g[k]$	Variations of $[Ca^{2+}]_o$ (μM)	

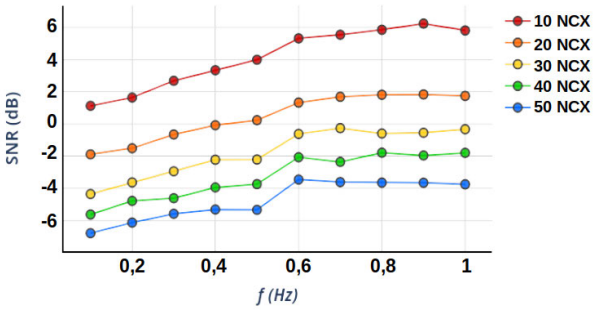

FIGURE 4. SNR analysis by number of NCX reactions.

First, it can be observed that the SNR grows as the frequency range increases since the higher the value of f, the more molecules of Ca^{2+} are introduced into the system in the same period, increasing $[Ca^{2+}]_i$ and, consequently, $X[k]$, which raises the SNR (Equation 10). However, from 0.6 Hz, the slope of the curves decreases, with more subtle variations as f increases, tending to become constant for all values of N_{NCX}. This behavior suggests that for higher frequencies, the energy of $g[k]$ increases proportionally to the signal's energy, causing the logarithmic curve to approach its horizontal asymptote.

From Figure 4, it is also possible to see that the SNR decreases with the increase of N_{NCX}. This happens because, with the increase in exchanges with the extracellular medium due to the action of the NCX, which is in reverse mode, $g[k]$ increases proportionally. However, it can also be observed that the SNR curves become less spaced from each other for higher values of N_{NCX}, for any value of f, resulting in a kind of saturation zone, or that is, the SNR tends to vary more discreetly after a certain number of NCX reactions, making

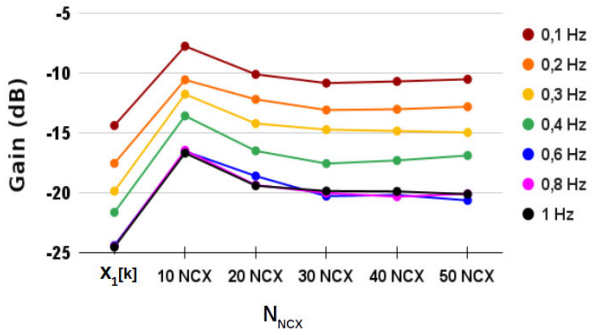

FIGURE 5. Average communication gain per number of NCX reactions.

the curve of $N_{NCX} = 10$ NCX an outlier of the analyzed sample space.

Similarly, analyzing the average $[Ca^{2+}]_i$ gain (Equation 13) illustrated in Figure 5, it is possible to see that this decreases with increasing f and N_{NCX}. This behavior happens because the increase in the frequency of $S[k]$ implies a more significant introduction of $[Ca^{2+}]_i$ in Tx, which is increasingly different from the concentration in Rx, increasing the relationship described in Equation 13. Similarly, the increase in N_{NCX} also increases the levels of $[Ca^{2+}]_i$ in Rx, reducing the difference about Tx. Furthermore, it is essential to point out that the gain obtained for the channel composed solely by the signaling of Ca^{2+} ($X[k] = x_1[k]$, only c_1 closed) presented the lowest value for their respective values of f.

Again, $N_{NCX} = 10$ NCX stood out from the others, presenting the highest gain for all values of f. For this reason, to avoid selecting an outlier, the next value of N_{NCX} (20 NCX) was chosen to perform the system analysis according to the metrics described in the following sections.

A. SIGNAL-TO-NOISE RATIO ANALYSIS

The signal-to-noise ratio (SNR) of the molecular communication system developed compares the level of $X[k]$ to the level of $g[k]$, in dB, which comes from the molecular reactions resulting from the action of the structures transport. Therefore this analysis does not apply to the channel composed purely of Ca^{2+} signaling. Figure 6 sketches the SNR obtained for the channel compositions, including the transport structures.

It is possible to see that increasing the frequency of $S[k]$ decreases the interference of $g[k]$ in $X[k]$ since the SNR increases for all channel compositions, that is, the level propagated signal is greater than the amplitude of the noise that travels from the extracellular medium to the intracellular medium. This happens because the increase in f stimulates intercellular diffusion reactions (via GJ channels), propagating a greater volume of $[Ca^{2+}]_i$ as the Tx introduces more molecules in the system at the same time, increasing the transmission of $X[k]$. This does not mean, however, that the reactions of the structures decrease, but that the reactions of Ca^{2+} signaling increase. In addition, the saturation zone can also be observed in the result described in Figure 6, so that from 0.7 Hz, the SNR tends to be constant, indicating that above this value of f, the signal and noise start to grow proportionally. Analyzing the T_b, it can be said that this quantity's influence on the SNR's behavior is low since there was no significant variation between the curves for all the reaction models discussed.

Note also that when the only transport structure present is the NCX (Figure 6 **a)**), the SNR is higher (ranging from -1 dB to 4 dB), followed by the addition of the other structures (Figure 6 **b)**) and the addition of the Na^{+} flag (Figure 6 **c)**), ranging from -2 dB to 2 dB and -4 dB to 0 dB, respectively. This result indicates that the addition of NKP and CP increased the influence of noise since they favor exchanges with the extracellular environment, as well as the addition of Na^{+} signaling, which, together with NKP, contributes indirectly to the variation of $[Ca^{2+}]_i$.

B. BIT ERROR RATE ANALYSIS

Figure 7 shows the results obtained for the bit error rate (BER) for all proposed channel compositions about the input frequency (f), varying the duration time of textitbit(T_b). Initially, it is essential to point out that increasing the T_b favors the transmission and reception of bits 1 because by having a more significant time window for determining the bit in modulation and demodulation, the volume of Ca^{2+} trafficked in that time (C_b) will be greater and, consequently, greater will be the chance that the C_b exceeds the established concentration threshold (σ_0). Analogous reasoning can be applied to f since the frequency of $S[k]$ increases the C_b transmitted for the same period.

Figure 7 **a)** outlines the behavior of the BER for the channel composed purely of Ca^{2+} signaling and reflects the reasoning explained in the previous paragraph as it reveals that the error rate decreases with the increase of f and T_b, since favoring the transmission, and consequent reception, of bits 1 decreases the probability of the system confusing bits 0 for bits 1 and vice versa. It is also possible to see in Figure 7 **a)** that, for curves with $T_b \leq 8 \times 10^{-4}$ s, there is a change in behavior from the values of $f = 0.2$ Hz and $f = 0.3$ Hz, making these two frequency values the most critical points of the analysis.

When considering other reaction models, as can be seen in Figures 7 **b)**, **c)** and **d)**, an inversion of behavior occurs. For $T_b \leq 10^{-3}$ s, the BER is directly proportional to the input frequency, whereas these two quantities become inversely proportional for $T_b > 10^{-3}$ s. The addition of reaction models that allow the exchange of Ca^{2+} with the extracellular medium causes the interference of $g[k]$ in $X[k]$ so that the increase in $[Ca^{2+}]_i$ from exchanges with $[Ca^{2+}]_o$ decreases the flow of molecules from intercellular diffusion and directly depends on the molecular concentration difference between the cells. In other words, this decrease in the flow of $[Ca^{2+}]_i$ is translated as a delay in $X[k]$ since the time required for demodulation will be longer for C_b to be sufficiently large to overcome σ_0, increasing the probability that the bits will be interpreted as 0 on reception.

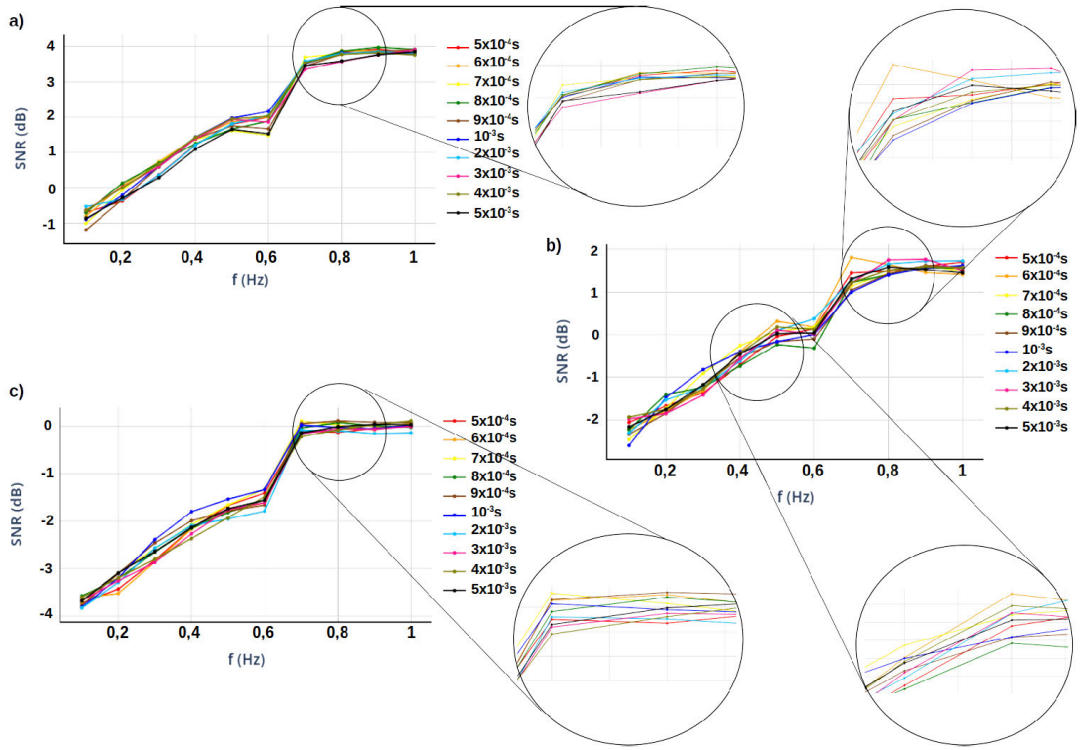

FIGURE 6. Signal-Noise Ratio by T_b for the channel compositions that are considered as ionic transport structures. a) c_1, c_2 and c_3 closed. b) c_1, c_3, c_4 and c_5 closed. c) All curly braces closed.

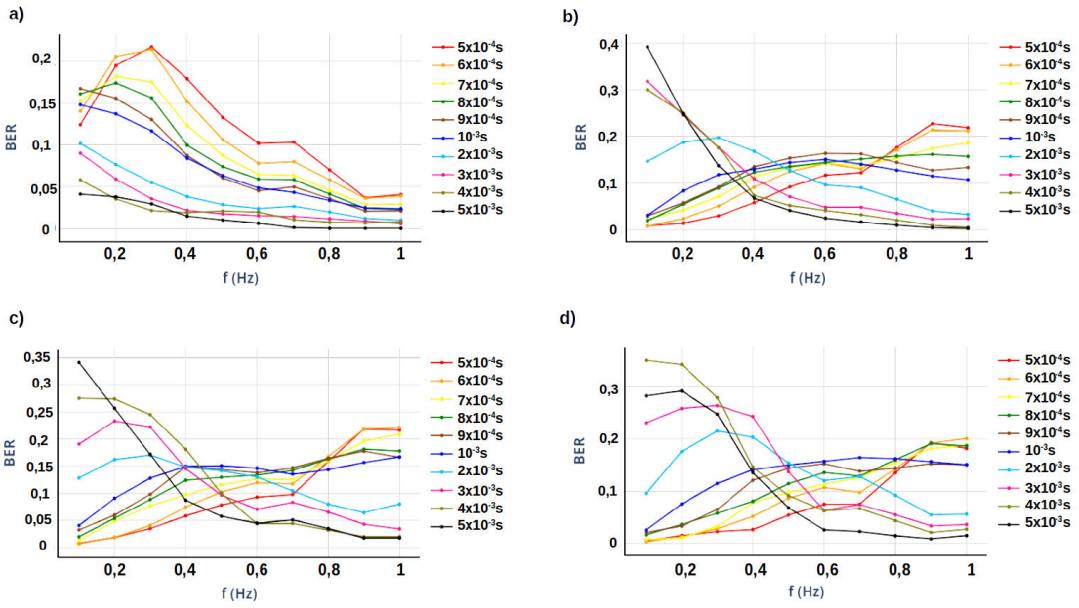

FIGURE 7. Signal-noise ratio by T_b for the channel compositions considered as ionic transport structures.

Thus, the result shown in Figures 7 **b)**, **c)** and **d)** reveals that below a certain value of T_b, the increase in the propagation of bits 1, due to the increase in frequency, causes more errors in reception, as the time window in the demodulation is not large enough to compensate for the delay in $X[k]$. For $T_b > 10^{-3}$ s, however, the time window starts to compensate for the interference effect, thus enabling greater detection of bits 1, so that the increase in frequency now lowers the error rate. This behavior transition also occurs with respect to f, since for $f < 0.4$ Hz, BER is directly proportional to T_b, while this proportionality is inverted for $f > 0.7$ Hz. The range of 0.4 Hz and 0.7 Hz can be considered a transition zone.

Furthermore, it can be seen in Figure 7 that the average error rate between the curves increased when adding the other

reaction models, due to the action of the noise $g[k]$ in the system, at the same time that similar behavior is observed between the curves of the combinations in which the ionic transport structures are considered.

C. CHANNEL CAPACITY ANALYSIS

The channel capacity, in turn, can be evaluated from Figure 8, which outlines this metric for all channels analyzed in this work. For the channel composed only by the signaling of Ca^{2+} (Figure 8 **a)**), it is possible to observe that the capacity is mostly decreasing with the increase of f, showing a change in behavior for values of T_b less than 3×10^{-3} s, since the curves belonging to this interval are directly proportional to the frequency of $S[k]$ when it is less than 0.4 Hz, approximately, and change that proportionality above that frequency value. For $T_b = 4\times10^{-3}$ s and $T_b = 5\times10^{-3}$ s, the channel capacity is always decreasing, whereas the curve of $T_b = 3 \times 10^{-3}$ s represents a transition state.

The behavior of decreasing the channel capacity with the increase of f can be explained because for a noise-free channel, where the error rate of bit is low, increasing the frequency of the input signal, although it reduces the BER (Figure 7 **a)**), it implies a decrease in the number of bits 0 trafficked in the system, reducing the total transmission rate and, consequently, the communication capacity of the system, since it depends on the transmission probability of both bits (Equation 20). The same happens for the time of bit so that the increase of this quantity reduces the total number of bits propagated since greater will be the C_b necessary for determining a single bit. When f is below 0.4 Hz, however, high BER causes increasing f to positively affect channel capacity for smaller values of T_b, as these make the system more susceptible to permutation between 0 and 1.

The same reasoning can be used to analyze the behavior of the channel capacity composed by the other reaction models. By observing the Figures 8 **b)**, **c)** and **d)**, it is possible to notice that the addition of transport structures to the system caused a change in proportionality between channel capacity and input frequency, making them directly proportional to the analyzed f range in almost all T_b curves. This result is justified by making a change in the analysis perspective so that in a scenario with the influence of noise, where the bit error rate is significant, increasing the frequency increases the channel capacity by decreasing the frequency. BER, overcoming the effect discussed in the previous paragraph.

It is important to note that, even if the channel capacity grows, its values, on average, did not exceed the results returned by the Ca^{2+} signaling channel since the numbers of the new models do not exceed 1 bps in all cases analyzed, reaching about 0.7 bps for Figures settings 8 **b)** and **d)**. Furthermore, the inversion in behavior for $T_b = 4 \times 10^{-3}$ s and $T_b = 5 \times 10^{-3}$ s starting at approximately 0.7 Hz suggests that from a given combination between T_b and f, the effect discussed for the channel composed purely by the signaling of Ca^{2+} becomes the determining factor in inverting the proportionality between f and the capacity of the channel, in which the signal and noise start to grow in the same proportion.

D. ANALYSIS OF COMMUNICATION GAIN

As for the communication gain, whose results are shown in Figure 9, the behavior of the curves is similar for all channel compositions, reflecting a decreasing exponential as the distance (r), in cells, between Tx and Rx increases. For example, figure 9 **a)** shows the gain of $[Ca^{2+}]_i$, according to Equation 13, for the channel composed only by the signaling of Ca^{2+}. It is observed that the gain decreases exponentially for $r < 3$ cells, becoming constant from this value onwards.

The decrease of approximately 150% for the higher frequency values reflects that as the distance from the receiver increases, the difficulty for the Ca^{2+} molecules to reach the desired destination also increases. That is, the $X[k]$ signal is attenuated. From $r = 3$ cells, however, the system enters a kind of saturation zone so that the attenuation of $X[k]$ has reached a value such that it is no longer affected by the increase in r. This saturation zone can also be perceived by analyzing the gain of about f, since the fall of approximately 2.5 dB, on average, is interrupted from $f = 0.6$ Hz, when the curves can be considered statistically equal.

As explained in the previous sections, increasing f increases the propagation of Ca^{2+} for the same period, allowing more information from $X[k]$ to be transmitted to Rx until, for a given value of f, the influence on the communication gain decreases, as the $[Ca^{2+}]_i$ in Tx rises in such a way that the increase in concentration in Rx is insignificant, in percentage.

With the addition of ion transport structures, whose results are shown in Figures 9 **b)**, **c)** and **d)**, the exponential behavior of the gain is expressed again. However, the percentage drop has decreased to around 60% at higher frequencies, showing flatter curves for $f = 0.1$ Hz. Furthermore, both saturation zones can also be perceived, and the order of the curves according to their frequency values. However, it is noted that the average gain value increased due to the first channel composition, reaching a maximum value of approximately -6 dB.

This result indicates that the addition of structures contributed to the increase of $[Ca^{2+}]_i$ in Rx, but does not necessarily reflect more excellent signal detection, since many molecules come from the extracellular medium and, therefore, are also a result of the noise interference $g[k]$, which also corroborates the more chaotic characteristic of the curves, since the variability of the system has increased.

E. COMPARISON BETWEEN CHANNEL COMPOSITIONS

Finally, Figure 10 shows the comparison of results between channel compositions for each evaluation metric. Figure 10 **a)** shows the BER for $T_b = 5 \times 10^{-3}$ s and shows that the addition of the other reaction models to a channel purely composed by signaling Ca^{2+} significantly increases the error rate, raising its maximum value from approximately 0.05 to approximately 0.35, although the exponential behavior is

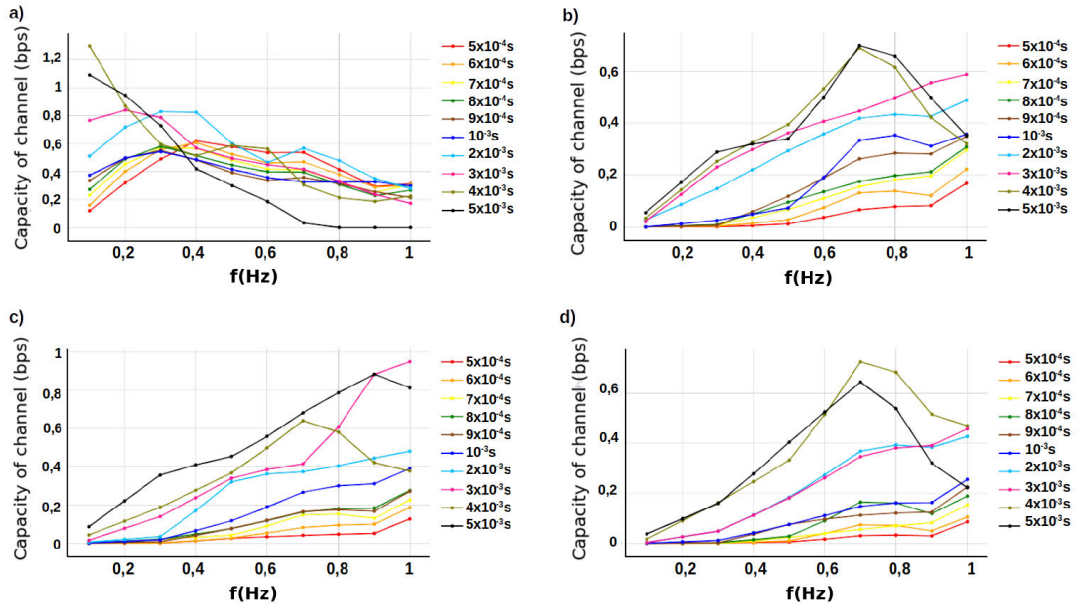

FIGURE 8. Channel capacity for each T_b reaction models.

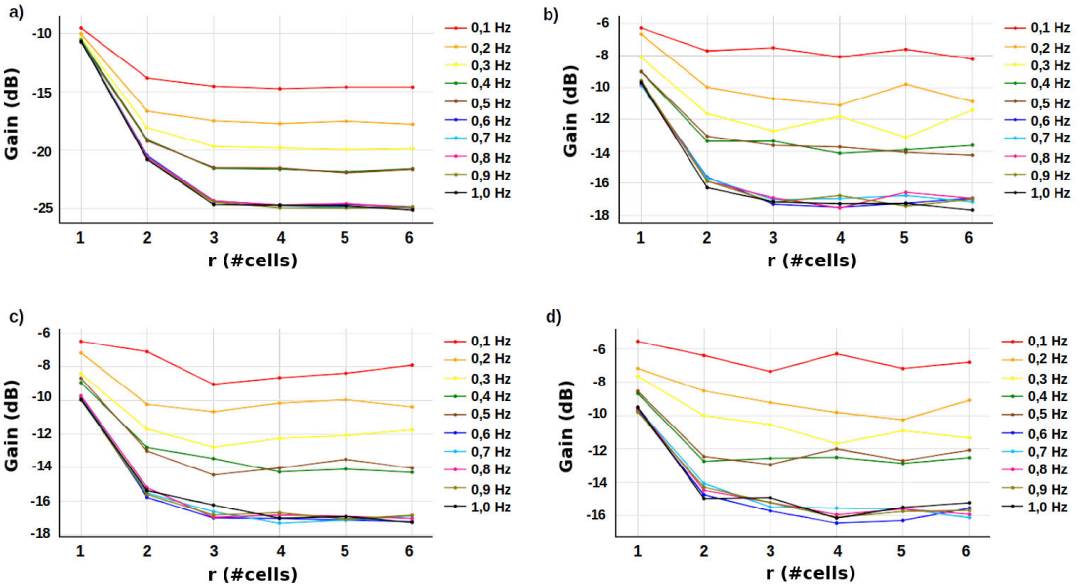

FIGURE 9. Communication gain per T_b for each combination of reaction models.

maintained and guarantees the approximation of the curve values from of 0.7 Hz, reaching approximately 0.

The behavior of the BER for the channels that include the transport structures is similar, as well as the values reached, with a slight difference in the error rate of the channel composed of all reaction models, which has a maximum value of 0.3, while the closed c_1, c_2 and c_3 configuration amounts to approximately 0.4. Thus, considering the variability of the communication system developed, the BER returned by the channels that include the structures can be considered statistically equal.

As for the channel capacity, represented in Figure 10 **b)** for $T_b = 5 \times 10^{-3}$ s, changing the channel composition allowed the analysis of this metric from a new perspective in a noisier scenario caused by the addition of structures, where the BER is high, the communication capacity becomes increasing, so that it is lower for $f < 0.4$ Hz and exceeds the configuration with only c_1 closed from that frequency value. Even so, the channel composed solely of Ca^{2+} signaling returned the highest channel capacity, with about 1.2 bps, while the channel configuration with c_1, c_3, Closed c_4 and c_5 (except for Na^{+} signaling) had approximately 0.9 bps as their

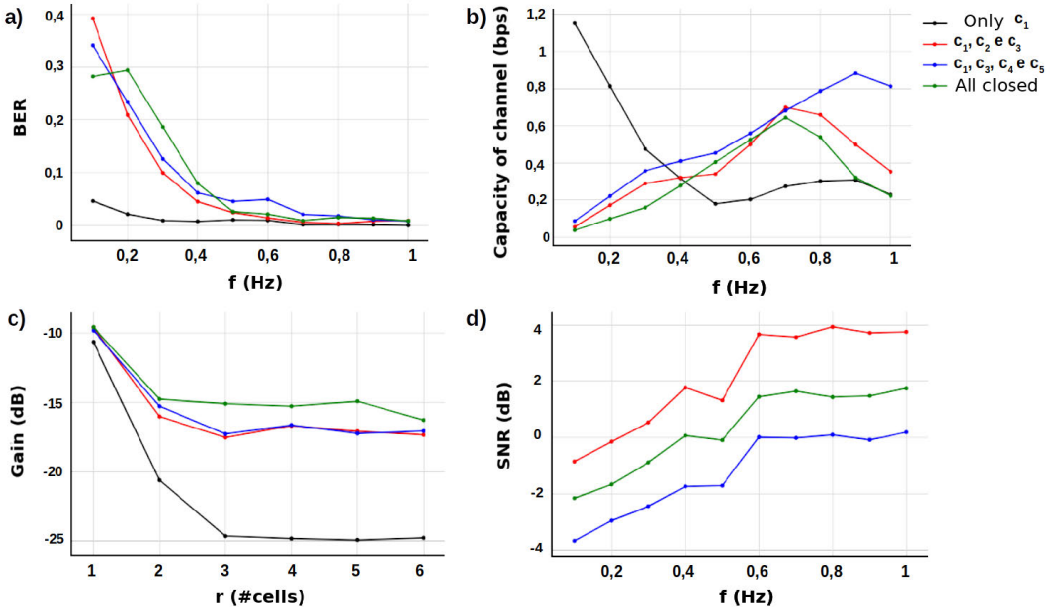

FIGURE 10. Comparison of channel composition results for each evaluation metric.

maximum value, distinguishing themselves from the other channel compositions that include the structures.

Figure 10 **c)** outlines the comparison of channels for the communication gain in $f = 1$ Hz, which reveals a considerable increase in this evaluation metric with the addition of the structure's carriage. However, since the gain is calculated considering the final average intracellular Ca^{2+} concentration in both Tx and Rx (Equation13), the values of $[Ca^{2+}]_i$ in Rx also represent the contribution coming from the exchanges with the extracellular medium, increasing the metric value, but not implying a more excellent detection of the signal itself by the Rx for these channel compositions. In any case, this result reveals the significant influence of the channel alteration on the communication system as a whole since the addition of the transport structures represented an average increase of approximately 30% in the levels of $[Ca^{2+}]_i$ from Rx. In addition, it is essential to highlight that the addition of Na^{+} signaling to the channel composition increased the gain by approximately 14.30%, on average.

Finally, the SNR, represented in Figure 10 **d)** for $T_b = 510^{-3}$ s, is fundamental to investigating the influence of the addition of structures on the system since it relates the signal to the noise produced by them. It is possible to observe that the channel composed of the transport structures without the Na^{+} signaling increased the noise influence by about 300%, on average, about the switch configuration that includes the NCX and the signaling (c_1, c_2 and c_3 closed). Considering all reaction models, however, there was an average reduction in the SNR of approximately 100%, showing that the signaling of Na^{+} caused a decrease in the influence of $g[k]$ on $X[k]$ against the closed c_1, c_3, c_4 and c_5 configuration. Thus, the addition of structures alone caused the greatest interference of extracellular noise in the signal.

VII. CONCLUSION

This paper proposed a molecular communication system in astrocyte tissue based on the dual relationship of Ca^{2+} and Na^{+}, through biological structures responsible for regulating concentration levels of ionic acid in this tissue, for evaluating the influence of these structures on the transmission of Ca^{2+}, as a reference molecule of the system. The communication gain, in turn, as well as the signal-to-noise ratio, made it possible to highlight the influence of noise on the Ca^{2+} signal since the first metric, for example, increased by about 30%, on average, due to the flow of molecules arising from exchanges with the extracellular medium. Our future includes increasing non-linear ionic transport also include spatial diversity, e.g. MIMO (Multiple Input Multiple Output).

REFERENCES

[1] J. Lallouette, M. De Pittà, and H. Berry, "Astrocyte networks and intercellular calcium propagation," in *Computational Glioscience*. Springer, 2019, pp. 177–210.
[2] C. R. Rose and J.-Y. Chatton, "Astrocyte sodium signaling and neurometabolic coupling in the brain," *Neuroscience*, vol. 323, pp. 121–134, May 2016.
[3] S. Kirischuk, V. Parpura, and A. Verkhratsky, "Sodium dynamics: Another key to astroglial excitability?" *Trends Neurosci.*, vol. 35, no. 8, pp. 497–506, Aug. 2012.
[4] V. Parpura and A. Verkhratsky, "Homeostatic function of astrocytes: Ca^{2+} and Na^{+} signalling," *Transl. Neurosci.*, vol. 3, no. 4, pp. 334–344, Jan. 2012.
[5] M. T. Barros, "Ca^{2+}-signaling-based molecular communication systems: Design and future research directions," *Nano Commun. Netw.*, vol. 11, pp. 103–113, Mar. 2017.
[6] M. T. Barros, P. Doan, M. Kandhavelu, B. Jennings, and S. Balasubramaniam, "Engineering calcium signaling of astrocytes for neural–molecular computing logic gates," *Sci. Rep.*, vol. 11, no. 1, p. 595, Jan. 2021.
[7] P. He, M. Su, Y. Cui, D. Wu, and R. Wang, "Epidemic-like calcium signaling in mobile molecular communication networks," *IEEE Trans. Nanobiosci.*, vol. 21, no. 3, pp. 425–438, Jul. 2022.
[8] G. Basso and M. T. Barros, "Biocomputing model using tripartite synapses provides reliable neuronal logic gating with spike pattern diversity," *IEEE Trans. Nanobiosci.*, vol. 22, no. 2, pp. 401–412, Apr. 2022.

[9] K. Lenk, B. Genocchi, M. T. Barros, and J. A. K. Hyttinen, "Larger connection radius increases hub astrocyte number in a 3-D neuron–astrocyte network model," *IEEE Trans. Mol., Biol. Multi-Scale Commun.*, vol. 7, no. 2, pp. 83–88, Jun. 2021.

[10] A. O. Bicen, I. F. Akyildiz, S. Balasubramaniam, and Y. Koucheryavy, "Linear channel modeling and error analysis for intra/inter-cellular Ca^{2+} molecular communication," *IEEE Trans. Nanobiosci.*, vol. 15, no. 5, pp. 488–498, Jul. 2016.

[11] A. Ahtiainen, B. Genocchi, J. M. A. Tanskanen, M. T. Barros, J. A. K. Hyttinen, and K. Lenk, "Astrocytes exhibit a protective role in neuronal firing patterns under chemically induced seizures in neuron–astrocyte co-cultures," *Int. J. Mol. Sci.*, vol. 22, no. 23, p. 12770, Nov. 2021.

[12] B. Genocchi, A. Ahtiainen, A. Niemi, M. Barros, J. Tanskanen, K. Lenk, J. Hyttinen, and N. Subramaniyam, "Astrocytes induce desynchronizing effects in neuron-astrocyte networks cultured on microelectrode arrays," Tech. Rep., 2023.

[13] M. T. Barros, S. Balasubramaniam, and B. Jennings, "Using information metrics and molecular communication to detect cellular tissue deformation," *IEEE Trans. Nanobiosci.*, vol. 13, no. 3, pp. 278–288, Sep. 2014.

[14] P. He, B. Pi, and Q. Liu, "Calcium signaling in mobile molecular communication networks: From a multimedia view," *IEEE Access*, vol. 7, pp. 164825–164834, 2019.

[15] A. R. Brazhe, A. Y. Verisokin, D. V. Verveyko, and D. E. Postnov, "Sodium–calcium exchanger can account for regenerative Ca^{2+} entry in thin astrocyte processes," *Frontiers Cellular Neurosci.*, vol. 12, p. 250, Aug. 2018.

[16] M. T. Barros, W. Silva, and C. D. M. Regis, "The multi-scale impact of the Alzheimer's disease on the topology diversity of astrocytes molecular communications nanonetworks," *IEEE Access*, vol. 6, pp. 78904–78917, 2018.

[17] N. Zhong, V. Beaumont, and R. S. Zucker, "Roles for mitochondrial and reverse mode Na^{+}/Ca^{2+} exchange and the plasmalemma Ca^{2+} ATPase in post-tetanic potentiation at crayfish neuromuscular junctions," *J. Neurosci.*, vol. 21, no. 24, pp. 9598–9607, Dec. 2001.

[18] W. G. Regehr, "Interplay between sodium and calcium dynamics in granule cell presynaptic terminals," *Biophysical J.*, vol. 73, no. 5, pp. 2476–2488, Nov. 1997.

[19] M. Egan, M. Kuscu, M. T. Barros, M. Booth, A. Llopis-Lorente, M. Magarini, D. P. Martins, M. Schäfer, and P. Stano, "Toward interdisciplinary synergies in molecular communications: Perspectives from synthetic biology, nanotechnology, communications engineering and philosophy of science," *Life*, vol. 13, no. 1, p. 208, Jan. 2023.

[20] M. Koenigsberger, R. Sauser, M. Lamboley, J.-L. Bény, and J.-J. Meister, "Ca^{2+} dynamics in a population of smooth muscle cells: Modeling the recruitment and synchronization," *Biophysical J.*, vol. 87, no. 1, pp. 92–104, Jul. 2004.

[21] D. Parthimos, D. H. Edwards, and T. M. Griffith, "Minimal model of arterial chaos generated by coupled intracellular and membrane Ca^{2+} oscillators," *Amer. J. Physiol.-Heart Circulatory Physiol.*, vol. 277, no. 3, pp. H1119–H1144, Sep. 1999.

[22] M. Taynnan Barros, S. Balasubramaniam, and B. Jennings, "Comparative end-to-end analysis of Ca^{2+}-signaling-based molecular communication in biological tissues," *IEEE Trans. Commun.*, vol. 63, no. 12, pp. 5128–5142, Dec. 2015.

[23] F. F. Bukauskas, A. Bukauskiene, M. V. L. Bennett, and V. K. Verselis, "Gating properties of gap junction channels assembled from Connexin43 and Connexin43 fused with green fluorescent protein," *Biophysical J.*, vol. 81, no. 1, pp. 137–152, Jul. 2001.

[24] J. Lallouette, M. De PittÃ, E. Ben-Jacob, and H. Berry, "Sparse short-distance connections enhance calcium wave propagation in a 3D model of astrocyte networks," *Frontiers Comput. Neurosci.*, vol. 8, pp. 1–18, Apr. 2014.

[25] C. R. Rose and C. Karus, "Two sides of the same coin: Sodium homeostasis and signaling in astrocytes under physiological and pathophysiological conditions," *Glia*, vol. 61, no. 8, pp. 1191–1205, Aug. 2013.

[26] J. Chatton, P. J. Magistretti, and L. F. Barros, "Sodium signaling and astrocyte energy metabolism," *Glia*, vol. 64, no. 10, pp. 1667–1676, Oct. 2016.

[27] S. Kirischuk, L. Héja, J. Kardos, and B. Billups, "Astrocyte sodium signaling and the regulation of neurotransmission," *Glia*, vol. 64, no. 10, pp. 1655–1666, Oct. 2016.

[28] G. Ghézali, G. Dallérac, and N. Rouach, "Perisynaptic astroglial processes: Dynamic processors of neuronal information," *Brain Struct. Function*, vol. 221, no. 5, pp. 2427–2442, Jun. 2016.

[29] J. P. Castillo, H. Rui, D. Basilio, A. Das, B. Roux, R. Latorre, F. Bezanilla, and M. Holmgren, "Mechanism of potassium ion uptake by the Na^{+}/K^{+}-ATPase," *Nature Commun.*, vol. 6, no. 1, p. 7622, Jul. 2015.

[30] H. Alle, A. Roth, and J. R. P. Geiger, "Energy-efficient action potentials in hippocampal mossy fibers," *Science*, vol. 325, no. 5946, pp. 1405–1408, Sep. 2009.

[31] B. C. Carter and B. P. Bean, "Sodium entry during action potentials of mammalian neurons: Incomplete inactivation and reduced metabolic efficiency in fast-spiking neurons," *Neuron*, vol. 64, no. 6, pp. 898–909, Dec. 2009.

[32] R. C. Reyes, A. Verkhratsky, and V. Parpura, "Plasmalemmal Na^{+}/Ca^{2+} exchanger modulates Ca^{2+}-dependent exocytotic release of glutamate from rat cortical astrocytes," *ASN Neuro*, vol. 4, no. 1, pp. 33–45, 2012.

[33] S. Paluzzi, S. Alloisio, S. Zappettini, M. Milanese, L. Raiteri, M. Nobile, and G. Bonanno, "Adult astroglia is competent for Na^{+}/Ca^{2+} exchanger-operated exocytotic glutamate release triggered by mild depolarization," *J. Neurochem.*, vol. 103, no. 3, pp. 1196–1207, Nov. 2007.

[34] D. Kilinc and O. B. Akan, "An information theoretical analysis of nanoscale molecular gap junction communication channel between cardiomyocytes," *IEEE Trans. Nanotechnol.*, vol. 12, no. 2, pp. 129–136, Mar. 2013.

[35] J. Langer, J. Stephan, M. Theis, and C. R. Rose, "Gap junctions mediate intercellular spread of sodium between hippocampal astrocytes in situ," *Glia*, vol. 60, no. 2, pp. 239–252, Feb. 2012.

[36] J.-Y. Chatton, P. Marquet, and P. J. Magistretti, "A quantitative analysis of L-glutamate-regulated Na^{+} dynamics in mouse cortical astrocytes: Implications for cellular bioenergetics," *Eur. J. Neurosci.*, vol. 12, no. 11, pp. 3843–3853, Nov. 2000.

[37] E. Syková and C. Nicholson, "Diffusion in brain extracellular space," *Physiological Rev.*, vol. 88, no. 4, pp. 1277–1340, Oct. 2008.

[38] S. Kadloor, R. S. Adve, and A. W. Eckford, "Molecular communication using Brownian motion with drift," *IEEE Trans. Nanobiosci.*, vol. 11, no. 2, pp. 89–99, Jun. 2012.

[39] J. Lytton, "Na^{+}/Ca^{2+} exchangers: Three mammalian gene families control Ca^{2+} transport," *Biochem. J.*, vol. 406, no. 3, pp. 365–382, Sep. 2007.

[40] D. Noble and A. Herchuelz, "Role of Na/Ca exchange and the plasma membrane Ca^{2+}-ATPase in cell function: Conference on Na/Ca exchange," *EMBO Rep.*, vol. 8, no. 3, pp. 228–232, Mar. 2007.

[41] G. M. Cooper, *The Cell: A Molecular Approach*, 2nd ed. 2000.

[42] S. Kirischuk, H. Kettenmann, and A. Verkhratsky, "Na^{+}/Ca^{2+} exchanger modulates kainate-triggered Ca^{2+} signaling in bergmann glial cells in situ," *FASEB J.*, vol. 11, no. 7, pp. 566–572, Jun. 1997.

[43] H. Rojas, C. Colina, M. Ramos, G. Benaim, E. H. Jaffe, C. Caputo, and R. DiPolo, "Na^{+} entry via glutamate transporter activates the reverse Na^{+}/Ca^{2+} exchange and triggers $Ca(i)^{2+}$-induced Ca^{2+} release in rat cerebellar type-1 astrocytes," *J. Neurochem.*, vol. 100, no. 5, pp. 1188–1202, Mar. 2007.

[44] M. P. Blaustein and W. J. Lederer, "Sodium/calcium exchange: Its physiological implications," *Physiological Rev.*, vol. 79, no. 3, pp. 763–854, Jul. 1999.

[45] L. Beaugé and R. DiPolo, "Effects of monovalent cations on Na–Ca exchange in nerve cells," *Ann. New York Acad. Sci.*, vol. 639, nos. 1, pp. 147–155, Dec. 1991.

[46] M. Ottolia, N. Torres, J. H. B. Bridge, K. D. Philipson, and J. I. Goldhaber, "Na/Ca exchange and contraction of the heart," *J. Mol. Cellular Cardiology*, vol. 61, pp. 28–33, Aug. 2013.

[47] K. S. Ginsburg, C. R. Weber, and D. M. Bers, "Cardiac Na^{+}–Ca^{2+} exchanger: Dynamics of Ca^{2+}-dependent activation and deactivation in intact myocytes," *J. Physiol.*, vol. 591, no. 8, pp. 2067–2086, Apr. 2013.

[48] D. Nicholls and S. Ferguson, "Quantitative bioenergetics (chapter 3): The measurement of driving forces," in *Bioenergetics*, 4th ed. 2013, pp. 27–51.

[49] M. T. Barros and S. Dey, "Feed-forward and feedback control in astrocytes for Ca^{2+}-based molecular communications nanonetworks," *bioRxiv*, 2017. [Online]. Available: https://www.biorxiv.org/content/early/2017/08/18/177154

[50] M. S. Kuran, H. B. Yilmaz, T. Tugcu, and I. F. Akyildiz, "Modulation techniques for communication via diffusion in nanonetworks," in *Proc. IEEE Int. Conf. Commun. (ICC)*, Jun. 2011, pp. 1–5.

[51] V. Jamali, A. Ahmadzadeh, C. Jardin, H. Sticht, and R. Schober, "Channel estimation for diffusive molecular communications," *IEEE Trans. Commun.*, vol. 64, no. 10, pp. 4238–4252, Oct. 2016.
[52] D. T. Gillespie, "Exact stochastic simulation of coupled chemical reactions," *J. Phys. Chem.*, vol. 81, no. 25, pp. 2340–2361, Dec. 1977.
[53] K. Thurley, L. F. Wu, and S. J. Altschuler, "Modeling cell-to-cell communication networks using response-time distributions," *Cell Syst.*, vol. 6, no. 3, pp. 355–367, Mar. 2018.
[54] L. Shi and L. Yang, "Error performance analysis of diffusive molecular communication systems with on-off keying modulation," *IEEE Trans. Mol., Biol. Multi-Scale Commun.*, vol. 3, no. 4, pp. 224–238, Dec. 2017.
[55] B. H. Koo, H. B. Yilmaz, C. Chae, and A. Eckford, "Detection algorithms for molecular MIMO," in *Proc. IEEE Int. Conf. Commun. (ICC)*, Jun. 2015, pp. 1122–1127.
[56] T. Nakano and J.-Q. Liu, "Design and analysis of molecular relay channels: An information theoretic approach," *IEEE Trans. Nanobiosci.*, vol. 9, no. 3, pp. 213–221, Sep. 2010.
[57] M.-J. Moore, T. Suda, and K. Oiwa, "Molecular communication: Modeling noise effects on information rate," *IEEE Trans. Nanobiosci.*, vol. 8, no. 2, pp. 169–180, Jun. 2009.
[58] Y. B. Band and Y. Avishai, *Quantum Mechanics With Applications to Nanotechnology and Information Science*. New York, NY, USA: Academic, 2013.
[59] P. Abshire and A. G. Andreou, "Capacity and energy cost of information in biological and silicon photoreceptors," *Proc. IEEE*, vol. 89, no. 7, pp. 1052–1064, Jul. 2001.
[60] M. T. Barros and S. Dey, "Set point regulation of astrocyte intracellular Ca^{2+} signalling," in *Proc. IEEE 17th Int. Conf. Nanotechnol. (IEEE-NANO)*, Jul. 2017, pp. 315–320.
[61] A. Vogt, A. Silapetere, C. Grimm, F. Heiser, M. Ancina Möller, and P. Hegemann, "Engineered passive potassium conductance in the KR2 sodium pump," *Biophysical J.*, vol. 116, no. 10, pp. 1941–1951, May 2019.
[62] F. Wang, N. A. Smith, Q. Xu, T. Fujita, A. Baba, T. Matsuda, T. Takano, L. Bekar, and M. Nedergaard, "Astrocytes modulate neural network activity by Ca^{2+}-dependent uptake of extracellular K^{+}," *Sci. Signaling*, vol. 5, no. 218, p. ra26, 2012.

CARLOS DANILO MIRANDA REGIS received the Ph.D. degree in electrical engineering with an emphasis in signal processing from the Federal University of Campina Grande. He is a Professor with the Federal Institute of Education, Science and Technology of Paraíba—IFPB, where he is also a Leader of the Digital Signal Processing Group (GPDS). His research interests include video and image processing and biological signal processing.

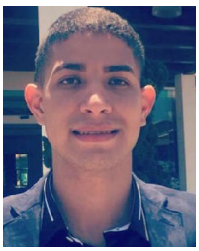

ÍTTALO DOS SANTOS SILVA received the B.Sc. and M.Sc. degrees in electronic engineering from the Federal Institute of Education, Science and Technology of Paraíba—IFPB, Brazil, in 2019 and 2022, respectively.

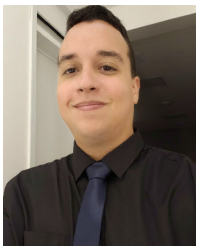

PEDRO IVO ARAGÃO GUIMARÃES received the B.Sc. degree in electronic engineering from the Federal University of Campina Grande—UFCG, Brazil, in 2021. He is currently pursuing the M.Sc. degree in electronic engineering with the Federal Institute of Education, Science and Technology of Paraíba—IFPB, Brazil.

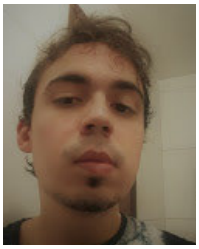

EMANUEL THIAGO DE ANDRADE DA SILVA is currently pursuing the B.Sc. degree in electronic engineering with the Federal Institute of Education, Science and Technology of Paraíba—IFPB, Brazil.

MICHAEL TAYNNAN BARROS (Member, IEEE) received the Ph.D. degree in computer science from South East Technological University, Ireland, in 2016.

He has been an Assistant Professor (a Lecturer) with the School of Computer Science and Electronic Engineering, University of Essex, U.K., since June 2020. He held multiple academic positions with prestigious grants in the Tampere University, Finland [Marie Skłodowska-Curie Individual Fellowship (MSCA-IF)]; and the Waterford Institute of Technology, Ireland (IRC GOI Postoc). He is also the Head of the Unconventional Communications and Computing Laboratory, which is part of the Communications and Networks Research Group. He received the European Commission's MSCA-IF, from 2019 to 2021; the Irish Research Council's (IRC) Government of Ireland Postdoctoral Fellowship, from 2016 to 2018; and the Enterprise Ireland's (EI) Commercialization Funding, from 2018 to 2019. He has over 80 peer-reviewed scientific publications in top journals and conferences, such as *Nature*, *Scientific Reports*, IEEE TRANSACTIONS ON COMMUNICATIONS, and IEEE TRANSACTIONS ON VEHICULAR TECHNOLOGY, in the areas of molecular and unconventional communications, biomedical engineering, bionano science, and beyond 5G.

Dr. Barros received the CONNECT Prof. Tom Brazil Excellence in Research Award, in 2020. Since 2020, he has been a Review Editor of the *Frontiers in Communications and Networks*, in the area of unconventional communications. He also served as the Guest Editor for the IEEE TRANSACTIONS ON MOLECULAR, BIOLOGICAL AND MULTI-SCALE COMMUNICATIONS.